Indian Journal of Chemical Technology
Vol. 33, March 2026, pp. 149-169
DOI: 10.56042/ijct.v33i2.25734

A novel Iraqi *Prunus Domestica* gum and lignin as natural precursors for the development of hydrogels for the slow release of thiamethoxam

Majeed A. Shaheed, Manu Nandal, Devendra Kumar & Rajinder K. Gupta*
Department of Applied Chemistry, Delhi Technological University, Pin-110042, Delhi, India
*E-mail:rkg67ap@yahoo.com

Received 20 November 2025; accepted 24 February 2026

Sustainability, which addresses the challenges of agricultural issues, requires the development of hydrogel-based systems. For this purpose, new hydrogels have been synthesized via free radical copolymerization using Iraqi *Prunus domestica* gums (IPDG) and lignosulfonic acid sodium salt (LS), and were analyzed by FTIR, ^{13}C NMR, FESEM, XRD, and TGA techniques. The swelling capacities are 165.357 g.g^{-1} of LS-IPDG-g-SAH, 159.267 g.g^{-1} of LS-g-SAH, and 156.469 g.g^{-1} of IPDG-g-SAH hydrogel formulations. The pH 7.2 exhibited the maximum swelling in distilled water compared to alkali and acidic media. The release behaviour of thiamethoxam in distilled water has been modeled using the Korsmeyer–Peppas, Weibull, and Higuchi models. Up to 92 h, 27.793%, 25.447%, and 23.538% of the pesticide are released from LS-IPDG-g-SAH, LS-g-SAH, and IPDG-g-SAH, respectively. For soil application, the trend of water evaporation is in the decreasing sequence: blank soil > IPDG-g-SAH >LS-g-SAH >LS-IPDG-g-SAH after 12 days. These results generally present the prospects of hydrogels as environmentally friendly materials for agrochemical applications, providing opportunities for the controlled delivery of pesticides and increased resource efficiency. Additionally, the novel approach by incorporating IPDG and lignin-based hydrogels makes it of fantastic value in the field of potential agricultural development.

Keywords: Hydrogel, Iraqi *Prunus domestica*gums (IPDG), Lignin, Lignosulfonic acid sodium salt, Thiamethoxam

Introduction

In recent times, agricultural sustainability has continued to face increasing challenges on a global scale, primarily due to water scarcity, soil degradation, inadequate fertilizer use, and environmental contamination[1]. One of the most significant reasons behind these is the increased loss of nutrients, irregular rainfall, climate change, and droughts[2]. Additionally, the increased wastage of agricultural chemicals leads to the loss of nutrients through leaching, runoff, and volatilization, resulting in lower crop productivity and reduced soil fertility[3].

To overcome the challenges under real field conditions, focus must be placed on developing new biodegradable materials at a low cost that surpasses the efficiency of renewable materials, such as smart hydrogels[4]. In addition, the search for new raw materials continues to enhance the effectiveness of smart hydrogels in controlling the release of agrochemicals and preserving soil moisture, thereby enhancing agricultural production[5].

A hydrogel is a specific kind of hydrophilic polymer that is physically or chemically crosslinked. It consists of an interconnected network that is capable of swelling by absorbing large amounts of water and other aqueous fluids. Bio-based precursors have recently garnered growing interest in recent times[6]. In general, most hydrogels are produced from polysaccharides, which contain multiple hydroxyl groups that can be modified to create smart materials. These properties make the polysaccharide-based hydrogels (IPDG) suitable for various agrochemical applications[7]. This work enables controlled release, retains water with intrinsic nutrients, and reduces nutrient dispersion and poor soil health in real field conditions[8].

Hydrogels have been prepared from natural and synthetic precursors, including starch, cellulose, poly(acrylamide), poly(acrylic acid), and alginate, as reported in previous studies[9]. High production costs, unsatisfactory biodegradability, and inadequate mechanical strength make the application of hydrogels limited under practical conditions[10]. Specifically, placing the main emphasis on plant resources rather than on petrochemical feedstock will contribute to the circular economy, including low-cost natural polymers from agricultural by-products or forest by-products[11].

Previous studies have highlighted that hydrogel-based materials, obtained by combining fertilizer nutrients with hydrogels either chemically or physically, can significantly reduce the environmental impact of traditional fertilizers by minimizing volatilization loss and serving irrigation events. These materials have been referred to as a "mini-reservoir" and act to swell in aqueous media due to their ability to absorb substantial amounts of water and nutrients and their controlled release over a period of time[12]. They are also used as plant growth regulators and in seed coating formulations for enhancing germination and establishment in seedlings under field conditions for agricultural applications[13].

Prunus domestica gum, from the *Rosaceae* family, is one among the natural polymers obtained from the exudates of tree trunks when plants are subjected to diseases or extreme external environmental conditions. It is soluble in warm water, which results in a viscous colloidal solution with no odour and no taste. This biopolymer consists of heterogeneous complexes of polysaccharides with simple monosaccharides such as galactose, arabinose, mannose, and rhamnose, along with uronic acid, which imparts its hydrophilic character and film-forming capability[14]. This type of natural polymer exhibits very good biocompatibility and biodegradability and has thus gained increasing importance in pharmaceutical formulations, medicinal preparations, cosmetics, and as a stabilizing agent in the food industry[15].

Similarly, Lignin is also another type of natural, renewable polymer, considered the chief source of soil organic matter, and it consists of aliphatic hydroxyl, phenolic, methoxycarbonyl, and carboxyl active functional groups. It has been recognized for its importance in promoting water-holding capacity and improving soil quality, as well as for its value as an attractive raw material for the synthesis of slow-release fertilizers[16]. Lignin is the second most abundant compound in lignocellulosic biomass, accounting for about 15-35% of its composition. It is considered one of the most abundant organic compounds on Earth, with approximately 100 million tons produced annually as a waste product of the bioethanol and paper manufacturing industries[17]. These biofertilizers have generated interest in plant growth promotion by chelation of nutrients in a complex, cross-linked three-dimensional network. It can be used in grafting with *Prunus domestica* gums (PDG) in the synthesis of hydrogels. This component is a crucial part of the plant cell wall, primarily found in wood and bark, and is closely associated with hemicellulose and cellulose. It is mainly composed of aromatic monomers commonly known as monolignols, which correspond to para-coumaryl alcohol, coniferyl alcohol, and sinapyl alcohol. The complex structure provides mechanical strength and resistance to microbial attack through strong carbon-carbon and carbon-oxygen-carbon ether bonds; hence, it is an integral and vital part of soil organic matter.

The incorporation of natural derivatives into hydrogel systems is a promising and multifunctional approach for their application in agriculture[18]. However, to date, no work has focused on the synthesis of hydrogels based on the grafting of Prunus domestica gums and lignin for agrochemical applications, especially under real soil and climatic conditions[2,3].

However, a substantial gap in research remains, with no work having been done on the hydrogels prepared from IPDG-grafted lignin specifically designed for agrochemical delivery. Although *Prunus armeniaca* gum has been incorporated into pH-responsive hydrogel systems[19] and *Prunus domestica* gum has been grafted with polyaniline for corrosion protection applications[20], the applicability of these gums to controlled pesticide release systems for agricultural purposes is largely unexplored. While several works have investigated the properties of hydrogels modified with lignin, this is the first study to compare different *Prunus domestica* gum and lignin-based hydrogels as carriers for thiamethoxam to the best of the authors' knowledge.

The work clearly demonstratesa novel formulation addressing various agricultural problems. This aims to mitigate the environmental impact of pesticide runoff into water bodies by releasing pesticides slowly, prolonging their release, and controlling their release, thereby minimizing ecological risks. Ultimately, the formulated hydrogels have the capability to reduce environmental impact and improve pesticide efficiency.

Experimental Section

Chemicals

In this research, the gum shown in Fig. 1 was manually collected from the trunks and branches of the IPDG tree (family *Rosaceae*) in Najaf, Iraq, in January 2025. The plant identity of the tree was

Fig. 1 — IPDG manually collected from Najaf, Iraq.

authenticated by Prof. Kadum Mohammed Abdullah and Prof. Zaid Khaleel Kadhim from the Karbala University Faculty of Agriculture, Iraq. Taxonomic authentication was also confirmed at the Department of Applied Chemistry, Delhi Technological University. lignosulfonic acid sodium salt (LS) (average Mol. wt.~52,000 with high water solubility) was imported from Sigma Aldrich. Acrylic acid (AA), Sodium Hydroxide (NaOH), and N,N-methylene bisacrylamide (MBA) were purchased from CDH Pvt Ltd. Potassium persulfate (KPS) was purchased from SD Fine Chem Ltd. The Institute of Pesticide Formulation and Technology, Gurugram, India, supplied the thiamethoxam for this research, which had a purity of 96.5%. All solutions necessary were prepared using distilled water (DW) as the aqueous medium for polymerization.

Synthesis of LS-IPDG-g-SAH, LS-g-SAH, and IPDG-g-SAH hydrogels

Copolymer hydrogels were synthesized by minutely modifying protocols described in previous reports[21]. All the synthesized formulations utilized various quantities of IPDG and LS as natural precursors. The initiation was carried out using KPS, and crosslinking was achieved with MBA through the free radical copolymerization method. The neutralization stage for the reaction mixture was performed at room temperature by adding 7.2 g of AA and 13 mL of 8.07 mol.L^{-1} NaOH. Afterward, the mixtures were stirred continuously at 400 rpm under atmospheric air for 3 h after adding KPS and MBA in different proportions. The reaction mixture was then poured into test tubes, and the heating process was achieved in a water bath at 60°C for one hour. Thereafter, the copolymerized hydrogels were cut into fine discs and soaked in DW for 24 h to remove any unreacted compounds. The constant weight for each hydrogel product was achieved after drying in a hot air oven (ACCUMAX India) at 60°C. The hydrogels were stored in a desiccator for future use. Initially, the amounts of IPDG and LS were varied for various formulations (Table 1) to obtain the optimized amount of both polymers for maximum swelling. Later, the formulation with maximum swelling index (SI) was used to prepare controls for IPDG and lignin-based hydrogels.

Characterization and properties of synthesized hydrogels

The functional groups of IPDG, LS, and the resulting hydrogels were identified using FT-IR spectroscopy. Characterization was performed using the KBr pellet technique on a Perkin Elmer 2000 FT-IR spectrometer at a resolution of 1 cm^{-1}. The scan was performed between 4000 and 500 cm^{-1} with a resolution of 1 cm^{-1}. Solid-state ^{13}C CPMAS NMR spectra of the samples were determined using a Bruker Ascend-400 spectrometer at a frequency of 400 MHz. FESEM on a Carl Zeiss instrument was employed to identify surface morphology. XRD analysis was carried out to analyze the crystallinity and amorphous nature of the material using a RIGAKU system with a Cu Kα source, operated at a voltage of 50 kV. The samples were placed in the specimen holder and scanned using a step size of 0.04° at a 5° (2θ/min) scanning speed between 5° and 80°. The thermal stability character of the hydrogel formulation was studied using a HITACHI STA300 TG/DTA. A controlled quantity of the sample powder was placed in an airtight sample container under a flow of 200 mL/min of nitrogen gas and heated at a rate of 5 °C/min from 35°C to 900°C.

Swelling experiment

The swelling study was performed to assess the water adsorption tendency of LS-IPDG-g-SAH, LS-g-SAH, and IPDG-g-SAH hydrogels. Initially, all the hydrogel samples were dried at 60°C until all moisture was eliminated entirely, weighed, and then soaked in DW at room temperature. The samples were withdrawn at certain periods, softly blotted using filter papers to remove excess water from the surface of the hydrogels, and weighed[22]. The swelling index (SI) was described and calculated using Eq. 1:

Table 1 — Formulations of hydrogels and their swelling index (SI)

Formulation code	Natural polymers		Monomer	Crosslinker	Initiator	SI ± SD ($g.g^{-1}$) after 80h
	LS (g)	IPDG (g)	AA(g)	MBA (g)	KPS (g)	
LS-IPDG-g-SAH1	0.100	0.100	7.56	0.08	0.1	115.326±1.678
LS-IPDG-g-SAH2	0.100	0.200	7.56	0.10	0.1	121.689±1.856
LS-IPDG-g-SAH3	0.100	0.300	7.56	0.12	0.1	87.843±0.867
LS-IPDG-g-SAH4	0.100	0.400	7.56	0.15	0.1	61.512±1.437
LS-IPDG-g-SAH5	0.200	0.100	7.56	0.20	0.1	66.468±1.805
LS-IPDG-g-SAH6	0.200	0.200	7.56	0.08	0.1	165.357±2.331
LS-IPDG-g-SAH7	0.200	0.300	7.56	0.14	0.1	74.111±1.123
LS-IPDG-g-SAH8	0.200	0.400	7.56	0.12	0.1	93.020±1.624
LS-IPDG-g-SAH9	0.300	0.100	7.56	0.12	0.1	120.933±0.964
LS-IPDG-g-SAH10	0.300	0.200	7.56	0.14	0.1	93.140±2.035
LS-IPDG-g-SAH11	0.300	0.300	7.56	0.08	0.1	128.488±1.256
LS-IPDG-g-SAH12	0.300	0.400	7.56	0.10	0.1	135.400±1.21
LS-IPDG-g-SAH13	0.400	0.100	7.56	0.14	0.1	106.469±1.255
LS-IPDG-g-SAH14	0.400	0.200	7.56	0.12	0.1	163.953±1.198
LS-IPDG-g-SAH15	0.400	0.300	7.56	0.10	0.1	127.691±1.317
LS-IPDG-g-SAH16	0.400	0.400	7.56	0.08	0.1	157.216±0.926
LS-g-SAH17	0.2	Nil	7.56	0.08	0.1	159.267±1.316
IPDG-g-SAH18	Nil	0.2	7.56	0.08	0.1	156.469±1.352

$$\mathrm{SI}(\mathrm{g}\cdot\mathrm{g}^{-1}) = \frac{\mathrm{W_O} - \mathrm{W_d}}{\mathrm{W_d}} \quad \ldots (1)$$

Here, W_0 and W_d denote the swollen and dry weight of the hydrogels, respectively.

Network parameters of LS-IPDG-g-SAH, LS-g-SAH, and IPDG-g-SAH hydrogels

The swelling data and the dimensions related to drying and swelling of polymers were used to calculate the network parameters of the synthesized LS-IPDG-g-SAH, LS-g-SAH, and IPDG-g-SAH hydrogels. The volume fraction of hydrogel, solvent interaction parameter, molar volume of solvent, swelling density, molecular weight of crosslinker, and hydrogel density in the dried state are parameters related to the Flory-Rehner model [23].

Volume fraction (ϕ)

The ratio of the volume of dried hydrogel (V_{H_d}) to the volume of swollen hydrogel (V_{H_s}) by water absorption is the volume fraction of hydrogel. Otherwise, the volume occupied by hydrogel represents the proportion of the overall area of the polymer, which can be determined using the given Eq. (2) [24].

$$\Phi = \frac{\mathrm{V_{H_d}}}{\mathrm{V_{H_s}}} \quad \ldots (2)$$

All the volumes of the hydrogel can be measured using a Vernier caliper model [25]. Both the volume of dry and swollen hydrogel is determined by multiplying the square of radius (r) by the height (h) of the cylindrical hydrogel discs, then multiplying that result by the mathematical constant (π), as per the given Eq. (3).

$$\mathrm{V} = \pi r^2 h \quad \ldots (3)$$

Hydrogel-solvent interaction (χ)

In order to evaluate hydrogel compatibility with the surrounding water, Eq. (4) was used for the computation of Hydrogel-solvent interaction parameters [24].

$$X = \frac{1}{2} + \frac{\Phi}{3} \quad \ldots (4)$$

Average molecular mass and density between crosslinks (Mc & d_{Hs})

The average masses of hydrogel chain segments located between two crosslinking points within the polymer network provides an insight on how tight or loose the network. When the volume of the fluid (V_w), the density (d_{Hs}), and the weight of the swollen hydrogel (W_{Hs}) are measured for the chains between two crosslinked points within a polymer network, these values can be used to calculate the average molecular mass of the hydrogel using specific Eqs (5) and (6) [26].

$$Mc = -\frac{\mathrm{d_{H_s}} \mathrm{V_w} (\Phi^{\frac{1}{3}} - \frac{1}{2}\Phi)}{\ln(1-\Phi) + \Phi + \mathrm{z}\Phi^2} \quad \ldots (5)$$

$$d_{H_s} = \frac{W_{H_s}}{V_{H_s}} \quad \ldots (6)$$

Crosslinking density (ρ)

The ability of packaging a three-dimensional network of polymeric chains is effectively evaluated by the degree of hydrogel chain crosslinking and the average molecular mass, as determined by the Eq. (7) [25].

$$\rho = \frac{d_{H_s}}{M_c} \quad \ldots (7)$$

Water evaporation of LS-IPDG-g-SAH, LS-g-SAH, and IPDG-g-SAH hydrogel and soil

The water retention capacity of soil treated with optimized hydrogels to prevent water evaporation was tested over 5 and 12 days. Multiple samples of hydrogel-treated soil (garden soil of DTU) and control were made using oven-dried soil (60°C, 72 h). 50mL of DW was added to every sample. The combined weight of the hydrogel-treated soil with water was measured as M_i. The samples were then left in the lab at room temperature and weighed daily, representing the weight as M_t[27]. In this study, the effects of LS-IPDG-g-SAH, LS-g-SAH, and IPDG-g-SAH on soil were determined by comparing the water evaporation rates of blank soil and hydrogel-treated soil. WE% was calculated using Eq. (8)[27].

$$WE\% = \frac{M_i - M_t}{M_i} x100 \quad \ldots (8)$$

Thiamethoxam loading and in vitro assessment of release

Dry preweighed samples of LS-IPDG-g-SAH, LS-g-SAH, and IPDG-g-SAH hydrogels were loaded with thiamethoxam by soaking them in a thiamethoxam solution (200 ppm) to enable the pesticide to adsorb on the hydrogels. The swollen hydrogels were taken out and dried to a constant weight. The release study added hydrogels (0.1 g) to a 200 mL beaker containing DW as the release medium for 24 h. The solution was kept at room temperature, and at set time intervals, 1 mL of solution was withdrawn, and the same volume of DW was added to preserve stoichiometry between the hydrogel and the solution[28]. The absorbance of thiamethoxam at 254 nm was measured using a UV-visible spectrophotometer, and the concentration of the solution was determined. The release ratio was obtained from the standard calibration curve as per Eq. (9)[29].

$$C\ (ppm) = \frac{A - 0.014}{0.04975} \quad \ldots (9)$$

Where C is the concentration of thiamethoxam in the aqueous solution (in ppm), A is the UV-visible absorbance value detected at 254 nm of the test sample.

Loading efficiency of thiamethoxam

The amount of thiamethoxam loaded into the formulations of LS-IPDG-g-SAH, LS-g-SAH, and IPDG-g-SAH hydrogels was estimated by comparing the total amount of pesticide present in each of the formulations with the residual thiamethoxam detected in the respective supernatants[30]. This approach facilitated the determination of pesticides loaded within the hydrogels. UV-visible spectrophotometer (Shimadzu, UV-1800) operating at a wavelength of 254 nm was utilized to perform the experimental analysis. Subsequently, a standard curve was applied to measure the thiamethoxam concentrations based on absorbance values. The loading efficiency (LE%) was defined using a predetermined equation, as presented in Eq. (10)[31].

$$LE(\%) = \frac{A_{total} - B_{free}}{A_{total}} x100 \quad \ldots (10)$$

Where A_{total} is the total amount of thiamethoxam in the stock solution before loading, and B_{free} is the residual amount of thiamethoxam remaining in the solution after the loading process.

Results and Discussions

Suggested mechanism for the formation of hydrogels

Practically, the lignosulfonate ions in aqueous solution, along with freely separated sodium ions, are produced upon dissolving LS in water. Suppose lignosulfonate ion is $HO - Lignin - SO_3^-$ and IPDG is R-IPDG-OH.

$$(HO - Lignin - SO_3^- Na^+)_n (Solid) \xrightarrow{H_2O} Na^+ + (HO - Lignin - SO_3^-)_n (Aqueous)$$

During the Initiation step, KPS molecules decompose to generate the sulfate radical anions(SO_4^{*-}) by breaking the O–O bonds [32]. These highly reactive radicals attack the natural precursors, leading to the formation of oxygen-generated radicals on lignosulfonate ions and IPDG through electron transfer and/or hydrogen abstraction mechanisms. Simultaneously, the active free radicals of sulfate react with the vinyl group of sodium acrylate, initiating the growth of poly(sodium acrylate) radical chains[33,34]. In the propagation step, the chain of each sodium acrylate radical continuously grows through

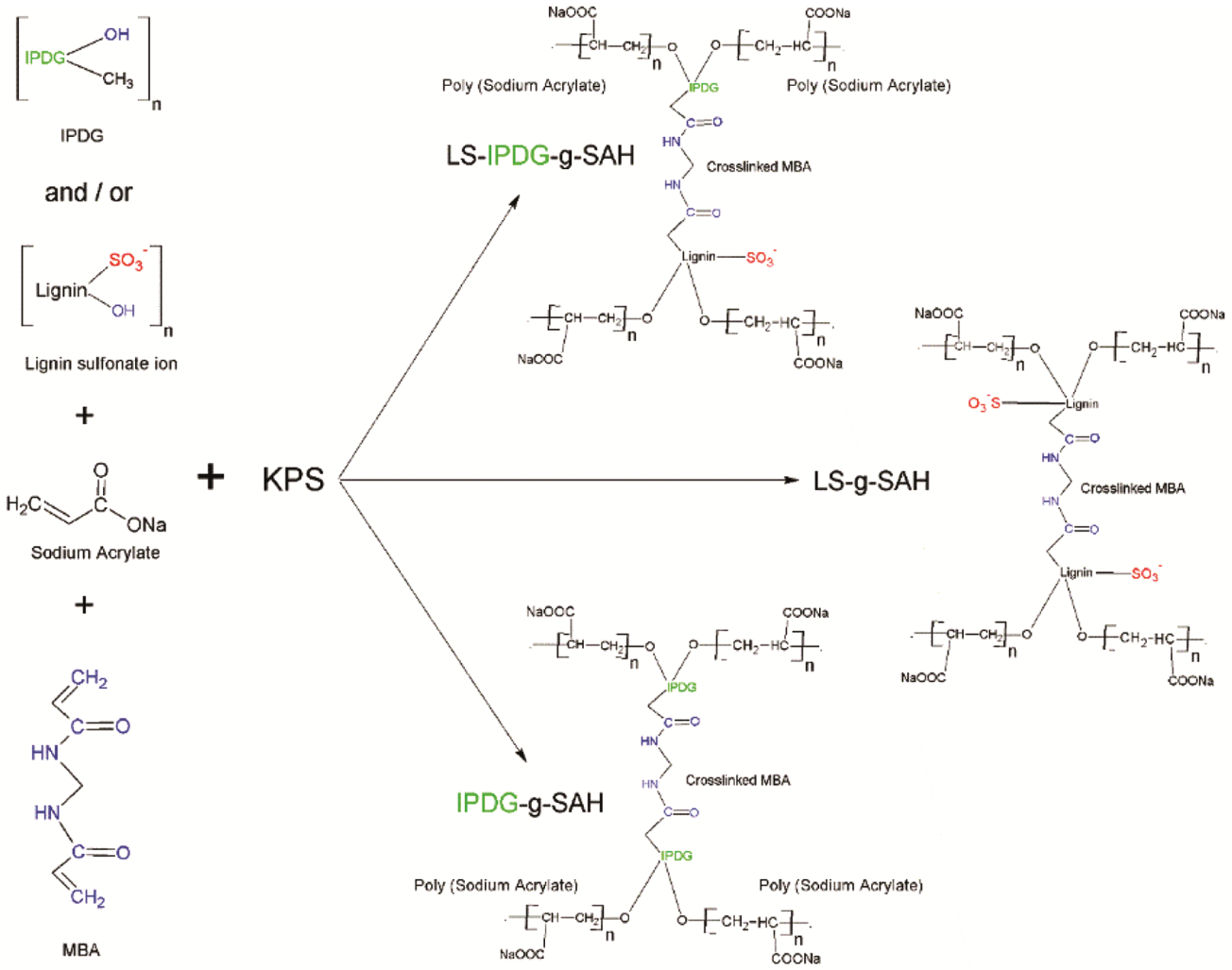

Scheme 1 — Suggested mechanism of IPDG-grafted lignin-based hydrogels

the successive addition of monomer units, formingan extended polymer chain[34]. The oxygen-generated radicals of lignosulfonate ions and IPDG further attack the vinyl groups of MBA and/or sodium acrylate monomers, resulting in the formation of a two-dimensional grafted polymer through ionic radical reactions. The multifunctionality of MBA then induces the formation of a three-dimensional polymer network via developing covalent interchain crosslinks [35]. Additionally, poly(sodium acrylate) radicals canreact with MBA molecules to produce a branched (2D) polymer through ionic radical pathways. During the termination step, two growing polymer radicals integrate, stopping chain propagation[36]. As a result, various hydrogels are created as three-dimensional networks of poly(sodium acrylate), lignin, and/or IPDG polymer chains, which extend and develop interchain crosslinking, with MBA serving as the crosslinking agent. The electrostatic repulsion between the negatively charged carboxylate ions spaced along the polymer chains expands the interlinked structure of the gel networks, thereby considerably increasing the hydrogel's ability to swell and absorb water[37]. The suggested mechanism is represented in Scheme 1.

Characterizations of Hydrogels

FT-IR spectroscopy

The FT-IR spectra of the pure IPDG, LS, and various samples (IPDG-g-SAH, LS-g-SAH, and LS-IPDG-g-SAH) of the synthesized hydrogels are illustrated in Fig. 2. The materials exhibit characteristic peaks between 500 and 4000 cm^{-1} related to various stretching and bending vibrations. The pure IPDG spectrum is depicted in Fig. 2 (a). A broad absorption band at ~3300 cm^{-1} is due to O–H

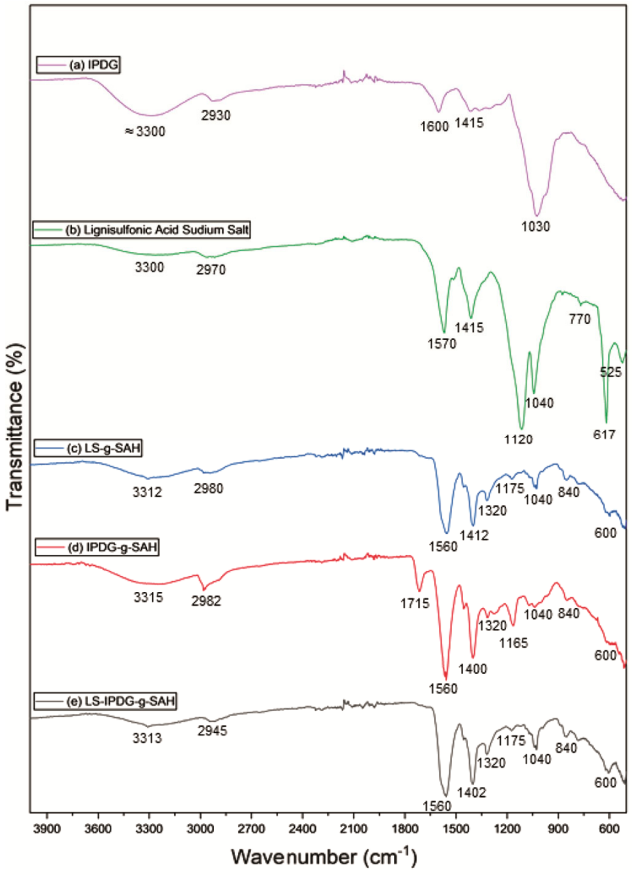

Fig. 2 — The FT-IR spectra of (a) pristine IPDG, (b) LS, and hydrogel formulation: (c) LS-g-SAH, (d) IPDG-g-SAH, and (e) LS-IPDG-g-SAH

stretching vibrations of hydroxyl groups, while the 2930 cm^{-1} peak is due to C–H stretching. The bands of characteristic shape at 1600 and 1415 cm^{-1} belong to asymmetric and symmetric stretching vibrations of carboxylate groups, while the intense band at 1030 cm^{-1} is due to C–O–C vibrations of glycosidic bond in the polysaccharides [14,38]. The broad band with low transmittance at 3300 cm^{-1} for LS in Fig. 2 (b), corresponds to the O–H stretching vibration, followed by the C–H stretching at 2970 cm^{-1}.The bands at 1570 and 1415 cm^{-1} are related to C=C aromatic stretching and aromatic ring C–H bending or symmetric COO^- stretching vibrations[39]. The sharp band at 1120 cm^{-1} indicates the presence of S=O or O–S–O stretching (sulfonate group), while the peak at 1040 cm^{-1} corresponds to the C–O–S stretching and SO_3^- symmetric or asymmetric vibration associated with sulfonate groups [40]. Notably, the absorption bands observed for LS at 1570 cm^{-1} and for IPDG at around 1600 cm^{-1} can be related to the typical vibration of the aromatic skeletal structure[41]. These findings suggest IPDG and LS are successfully grafted with AA. FTIR spectra, as shown in Figs 2 (c-e), comprise absorption bands at 3312 cm^{-1} for LS-g-SAH, 3315 cm^{-1} for IPDG-g-SAH, and 3313cm^{-1} for LS-IPDG-g-SAH, due to O–H stretching vibrations. Additional bands observed at 2970 cm^{-1}, 2980 cm^{-1}, and 2982 $cm^{-1}$are attributed to the stretching vibrations of the C–H bonds in $–CH_2$ and $–CH_3$, respectively[42]. Among the grafted copolymer formulations, the spectrum of the IPDG-g-SAH hydrogel shows a band at 1715 cm^{-1}. In contrast, in the case of LS-g-SAH and LS-IPDG-g-SAH, this band appears to disappear, indicating the presence of C=O stretching vibrations associated with ester or amide linkages of the MBA crosslinker[43,44]. The intense bands at 1560, 1400, 1402, and 1412 cm^{-1} are contributed by the asymmetric stretching in the carboxylate anion in the hydrogel structure. Though a minor change is seen in the peaks 1400 and 1320cm^{-1} are proposed for hydrogel formulation[45]. The similarity in the basic COO– peaks (1560 cm^{-1}) of the hydrogels' spectra highlights that the inherent structure is preserved, whereas grafting alters some chemical aspects[46]. The presence of extra bands at 1165 cm^{-1} for IPDG-g-SAH, 1175 cm^{-1} for LS-g-SAH and LS-IPDG-g-SAH, and 1040 cm^{-1} for all hydrogels corresponds to C–O–C stretching vibrations, indicating the successful grafting of acrylamide/acrylic acid units[35]. The fingerprint spectra were displayed within the range 500-1000 cm^{-1}. Finally, from the FT-IR spectra, it can be inferred that the hybrid LS-IPDG-g-SAH spectrum comprises a mixture of the major features of both IPDG and lignin, indicating the formation of ester linkages and providing evidence of successful copolymerization.

Solid-state ^{13}C CPMAS NMR analysis of hydrogels based on IPDG

This technique gives insights intothe chemical structure and structural characteristics of hydrogels and polymers. LS and IPDG spectra were studied along with synthesized LS-IPDG-g-SAH, LS-g-SAH, and IPDG-g-SAH hydrogels, as shown in Fig 3. In the spectrum of LS (Fig. 3a), several notable major peaks with different intensities were located approximately at 14.3−34.0 ppm for alkyl chain $–CH_3$ or $–CH_2$, a sharp peak at 56.4 ppm for methoxy ($–OCH_3$), 73.8−81.5 ppm for aliphatic carbons (Cγ–OH and Cα–O–Ar) attached to oxygen, 105 ppm for anomeric or carbohydrate carbon, 130 ppm for carbon condensed in aromatic ring(C–C), 147−153 ppm for

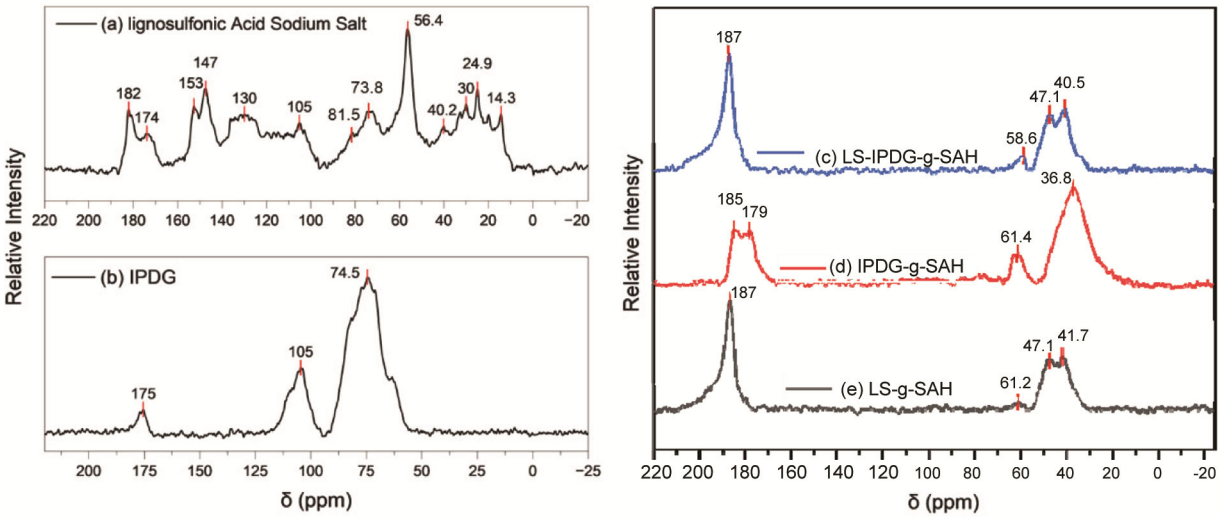

Fig. 3 — SS ^{13}C CPMASNMR spectrum of (a) LS, (b) IPDG, and hydrogel formulation:(c) LS-IPDG-g-SAH, (d)IPDG-g-SAH, and (e) LS-g-SAH

carbon bonded to oxygen (C–O–) or sulfonate group (C–SO_3^-), and 174−182 ppm for carbonyl or carboxyl carbon[47,48]. IPDG (Fig. 3b), characterized by peaks at around 74.5, 105, and 75 ppm, are assigned to carbon rings, anomeric signals of carbons bound to oxygen, and the carbonyl carbon of gums, respectively[49,50]. At 175 ppm, a small intensity peak was identified. In the case of all hydrogels, the peaks between 36.8−41.7 ppm are due to aliphatic carbon chains (−CH_2/−CH_3), the signals at 58.6−61.4 ppm confirm that poly sodium acrylate has bonded with grafted lignin and gums through MBA, resulting in a three-dimensional network polymer hydrogel. The peaks at 185−187 ppm may be precisely attributed to the free COOH groups and crosslinks in the synthesized hydrogels. In the case of IPDG-g-SAH (Fig. 3d), the appearance of a new signal at 179 ppmis related to carboxyl groups present in the backbone [51,52]. Meanwhile, most of the characteristic peaks of IPDG and LS peaks are incorporated into their respective hydrogels.

Field emission scanning electron microscope (FESEM) analysis

The surface features, morphology, and crystallinity, along with the corresponding EDX spectra, were analyzed and recorded at 20,000× magnification for HA-IPDG-g-SAH, HA-g-SAH, and IPDG-g-SAH hydrogels, as shown in Figs 4(a-i).The FESEM images of LS-IPDG-g-SAH (Fig. 4a) at low magnification revealed that the microstructures exhibited folds and grooves with a compact, continuous morphology and a dense surface, and were slightly wrinkled without large pores. The image of LS-IPDG-g-SAH (Fig. 4b) at higher magnification became more precise and more defined, showing microtextures and fine wrinkles. This highlights a layered surface with microcracks, which can promote a larger surface area and improved diffusion. The increasing magnification confirms a heterogeneous structure, considering that the grafting and blending between IPDG and lignin were successfully performed. This suggests an enhancement in the water absorption capacity and sustainable release behaviour of the hydrogels. A similar observation was reported in a study on agrochemical-controlled release behavior of copolymer hydrogel[53]. The image of LS-g-SAH (Fig. 4c) at low magnification appears cracked and uneven, presenting a dense, compact surface texture with a rough and irregularly shaped particle at the center. These features indicate partial aggregation and crosslinking density within the polymer matrix. Whereas, at higher magnification, image of LS-g-SAH (Fig. 4d) reveals that the surface has few visible pores and cracks, displaying a more compact and smoother morphology. These morphologies suggest a densely networked structure and a uniform hydrogel formed through the integration of sodium acrylate and lignosulfonate salts, which may reduce diffusion pathways leading to low efficiency in agrochemical applications[54]. Fig. 4(e) at low magnification for IPDG-g-SAH shows a surface morphology with a clearly irregular and partially crystalline structure, exhibiting multiple edges and aggregated clusters. This feature suggests the formation of compact domains within the hydrogel network and a high

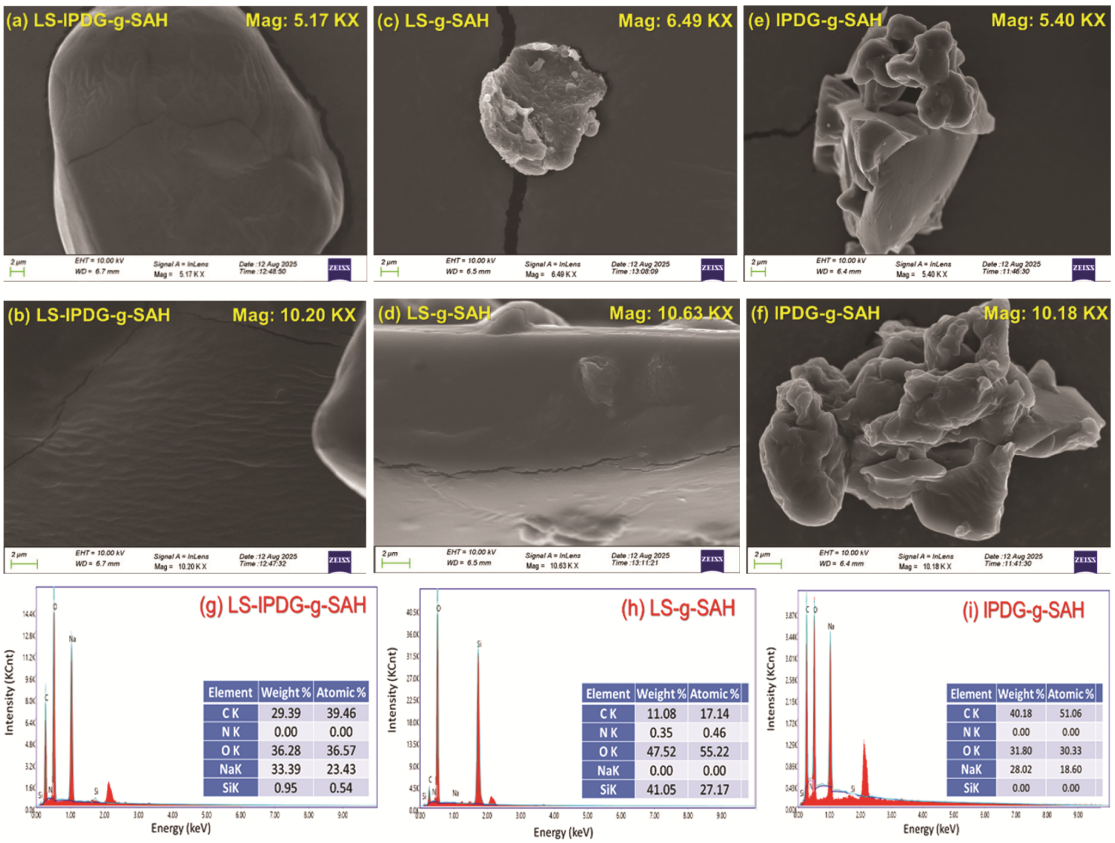

Fig. 4 — FESEM images of hydrogels: (a, b) LS-IPDG-g-SAHat magnifications of 5.17x and 10.20x; (c, d) LS-g-SAH at magnifications of 6.49x and 10.63x;(e, f) IPDG-g-SAHat magnifications of 5.40x and 10.18x. with corresponding EDX spectra in panels (g-i)

degree of crosslinking between IPDG and sodium acrylate, facilitated by the interaction of their functional groups. The image shows IPDG-g-SAH displaying a different morphology, characterized by oval and spherical particles, compact porosities, and irregular structures, suggesting strong aggregation within the hydrogel matrix. This compact morphology minimizes porosity compared to LS-IPDG-g-SAH and LS-g-SAH hydrogels, suggesting that IPDG-g-SAH may offer a more controlled release profile, making it highly favorable for sustained agricultural uses. Previous literature has reported that high porosity in conventionally formed hydrogels does not promote stronger intermolecular attractions, and vice versa [55]. The findings further demonstrate that increased porosity, resulting from a reduction in crosslinking density, facilitates the intermolecular attraction between the polymer and water molecules. Consequently, the stronger hydrogen bonding results from the increased proximity of polymer chains[56].

The EDX analysis was used to understand the potential enhanced properties of hydrogels, as well as to qualitatively and quantitatively analyze the minerals in the materials. The EDX spectra shown in Figs 4(g-i) determine the main elements (such as C, O, etc.) expected in the structure of hydrogels. The EDX spectra shown in Figs 4(g-i) revealed the dominant peaks of oxygen (36.57%, 55.22%, and 30.33%), nitrogen (0.00%, 0.46%, and 0.00%), and carbon (39.46%, 17.14%, and 51.06%) atoms, suggesting that the polymeric backbone of LS-IPDG-g-SAH, LS-g-SAH, and IPDG-g-SAH hydrogels, respectively, confirms the presence of organic polymer chains with high percent, consistent with a gum-based network[57]. Additionally, the trace amounts of N, Na, and Si indicated by inorganic peaks suggested the presence of mineral residue or natural components inserted during the grafting process, which alignswith the characteristics of the hybrid hydrogels[58]. The highest inorganic peaks in the EDX spectra of all hydrogels clearly explain the correlation with FESM micrographs, indicating the potential to improve mechanical strength and enhance water absorption capacity[59].

Thermogravimetric analysis (TGA)

Thermogravimetric analysis (TGA) is used to study the degradation behaviour of polymeric materials under thermal conditions. Fig. 5 shows the TGA plots of all prepared hydrogels, revealing four successive weight losses and a multi-step degradation profile within the 35–900°C range, indicating different structural components following a similar degradation pattern. The initial weight loss observed in the range of 35°C to 150°C for LS-IPDG-g-SAH and LS-g-SAH, and from 35°C to 190°C for IPDG-g-SAH, can be attributed to the evaporation of moisture and the volatilization of small-molecular compounds, resulting in mass losses of 14.4%, 18.8%, and 26.5% for LS-IPDG-g-SAH, LS-g-SAH, and IPDG-g-SAH, respectively. In the second stage, within the temperature ranges of 219–404°C, 236–408°C, and 200–411 °C, partial cleavage of side chains, degradation of carbohydrate backbones, and the decomposition of small ungrafted molecular polymers of IPDG and LS were observed. The corresponding mass losses in this range were 23.4%, 26.1%, and 39.5% for LS-IPDG-g-SAH, LS-g-SAH, and IPDG-g-SAH, respectively, which can be due to the decomposition of methylene, carboxylic, methyl, and alcoholic groups, along with carbohydrates derived from lignin and polysaccharide structures[19,60]. The highest thermal decomposition rate was recorded between approximately 410°C and 495°C for all samples. The third transition occurred in the range of 404–475 °C for LS-IPDG-g-SAH, 408–496°C for LS-g-SAH, and 411–490 °C for IPDG-g-SAH, showing mass losses of 43.9%, 48.3%, and 59.0% for LS-IPDG-g-SAH, LS-g-SAH, and IPD G-g-SAH, respectively, which could be attributed to the dissociation of bonds between the polymeric backbone of the monomer and cross-linker present in the hydrogel network[61]. Additionally, the slow degradation and subsequent stable phase between 510–730°C highlighted the enhanced thermal stability conferred by grafting two biopolymers to their respective hydrogels. At the end of the study, the last degradation phase occurs between 850°C and 900°C, indicating the breakdown of inert compounds. It can be suggested that the remaining mass percentage confirms the improvement in thermal stability achieved by incorporating IPDG and LS into the hydrogel network. A similar trend, indicating improvement in the thermal characteristics of the chemical transformation of lignosulfonates to lignosulfonamides, was reported by Komisarz *et al.*[62]. Notably, LS-IPDG-g-SAH, LS-g-SAH, and IPDG-g-SAH exhibited residual mass percent of 37.3 %, 42.5 %, and 23.5 %, respectively.

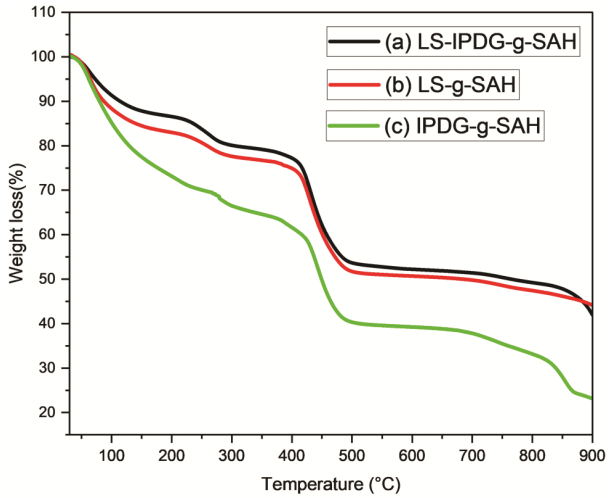

Fig. 5 — The TGA spectra of (a) LS-IPDG-g-SAH, (b) LS-g-SAH, and (c) IPDG-g-SAH hydrogels

XRD analysis

Fig. 6 presents the XRD diffractograms of (a) LS, (b) IPDG, (c) LS-IPDG-g-SAH, (d) LS-g-SAH, and

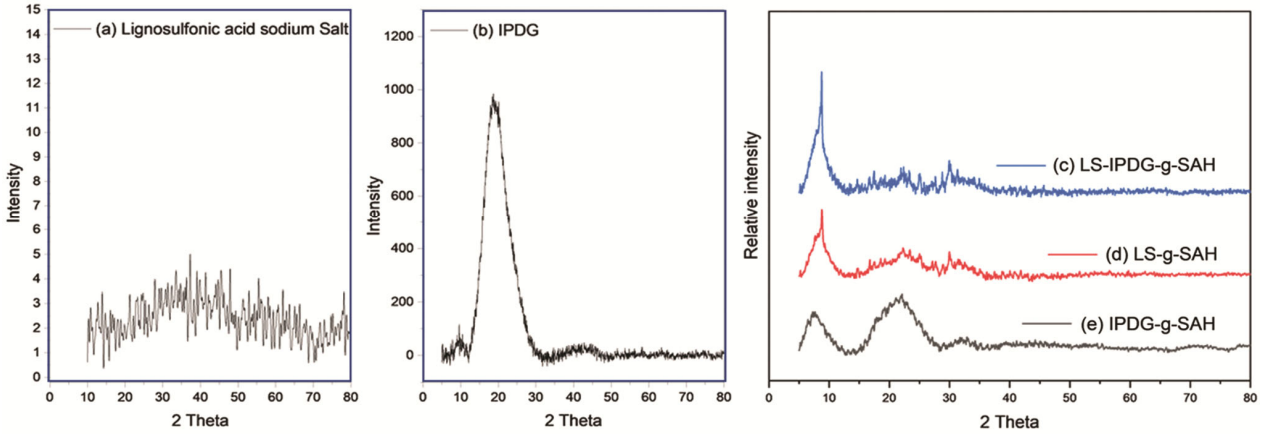

Fig. 6 — XRD patterns of (a) LS, (b) IPDG, and hydrogel formulation:(c) LS-IPDG-g-SAH, (d) LS-g-SAH and (e) IPDG-g-SAH

Table 2 — XRD-derived structural parameters (2θ, θ, Sinθ, and <R>) of the synthesized hydrogels

Hydrogel	2θ	θ	Sin θ	<R >
LS-IPDG-g-SAH	21.90	10.95	0.1900	4.40 Å
	29.92	14.96	0.2583	
LS-g-SAH	22.20	11.10	0.1927	4.35Å
	30.08	15.04	0.2596	
IPDG-g-SAH	22.28	11.14	0.1932	4.22Å
	32.42	16.21	0.2790	

(e) IPDG-g-SAH hydrogel formulations. This technique confirms the crystallinity, phase composition, and molecular interchain spacing within the hydrogel network chains, enabling researchers to determine whether the materials are amorphous or crystalline. The XRD pattern of LS in Fig. 6a shows several sharp, distinct peaks at different 2θ angles and various weak intensities. This indicates that the material is amorphous, confirming a non-crystalline nature, but small, weak features are inorganic residues[63]. In contrast, the XRD pattern of IPDG (Fig. 6b) exhibits a single broad peak positioned at approximately 2θ = 18.6°, characteristic of an amorphous structure lacking long-range ordered crystallinity in polysaccharide-based biomaterials[64,65]. This behaviour is typical of many natural gums and polymers, whose molecular chains are randomly arranged rather than organized in a repeating crystalline lattice. Other XRD spectra corresponding to the incorporation of IPDG and LS were observed in the patterns of LS-IPDG-g-SAH, LS-g-SAH, and IPDG-g-SAH hydrogels, as shown in Figs 6(c–e). The resulting XRD patterns reveal significant structural changes, highlighting the impact of grafting on the crystalline–amorphous equilibrium within the hybrid materials. Three distinct diffraction peaks were identified in the XRD pattern of LS-IPDG-g-SAH hydrogels, located at 2θ values of 8.70°, 21.90°, and 29.92°. These peaks exhibit sharp features with different intensities, indicating a partially crystalline structure. The presence of low-intensity peaks suggests limited crystallinity within the structure matrix. Regarding peak characteristics, LS-g-SAH is still present in the same manner but is noticeably less intense. This indicates that the crystallinity has decreased in the presence of the amorphous polymer (IPDG)[66], as shown bypeaks labelled c and d in Fig. 6.

IPDG-g-SAH hydrogel is an amorphous material, typically producing a broad, low-intensity signal in an XRD pattern, rather than sharp peaks. Thus, broad peaks occur due to the amorphous components of IPDG, which likely interfere with the crystalline order of LS, leading to smaller crystallite sizes and the formation of amorphous materials. This finding agrees with the comprehensive principle that incorporating an amorphous material with a crystalline material tends to reduce the overall crystallinity of the formulation[67].

Similar results have been reported for an amorphous polymer structure property, thereby supporting the material's non-crystalline nature[68,69]. Another result has also been attributed to grafting a natural polymer onto sodium acrylate[70]. Such amorphous structures are advantageous in hydrogel systems, as they typically favour water absorption, ion exchange, and molecular mobility, which are critical for agricultural and environmental applications[71]. The average molecular interchain spacing (<R>) of polymer chains in LS-IPDG-g-SAH, LS-g-SAH, and IPDG-g-SAH hydrogels has been calculated from the prominent diffraction peaks using Eq. 11[55].

$$< R >= \frac{5}{8}\left(\frac{\lambda}{sin\theta}\right) \quad \ldots (11)$$

where λ is the X-ray wavelength and θ is the diffraction angle at the maximum peak. The average molecular interchain spacing in different hydrogel formulations is presented in Table 2.

The <R> values reveal that LS-IPDG-g-SAH exhibits a larger interchain distance (4.40 Å), indicating an expanded network with weaker intermolecular interactions. Conversely, LS-g-SAH displays distances (4.35 Å), followed by IPDG-g-SAH, which presents smaller distances (4.22 Å), considering stronger intermolecular interactions with compact structures.

Swelling study of LS-IPDG-g-SAH, LS-g-SAH, and IPDG-g-SAH hydrogels

Fig. 7 presents the variations in the SI of all hydrogel systems in DW after time intervals. The SI of LS-IPDG-g-SAH was maximum (165.357±2.331 $g.g^{-1}$) at equilibrium after 80 h. LS-g-SAH had an SI of 159.267±1.316 $g.g^{-1}$ at 80 h, whereas IPDG-g-SAH had an SI of 156.469±1.352 $g.g^{-1}$after 80 h. Based on

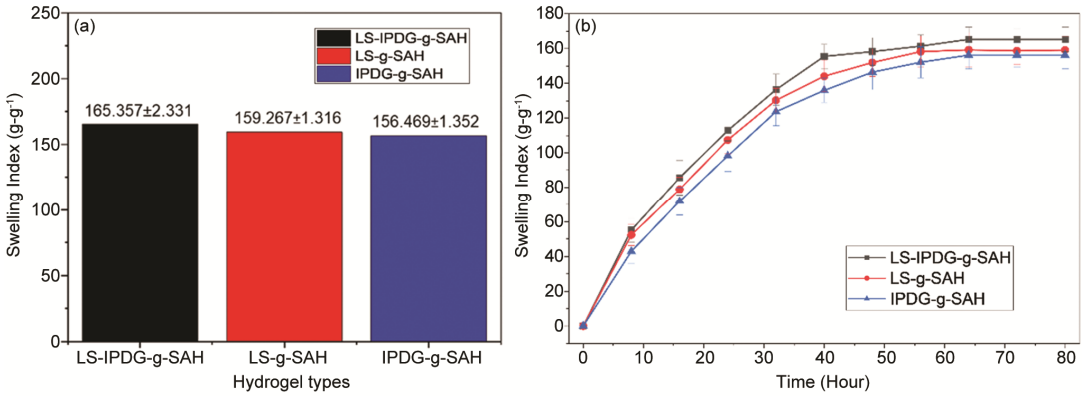

Fig. 7 — (a) Comparative swelling and (b) concerning time

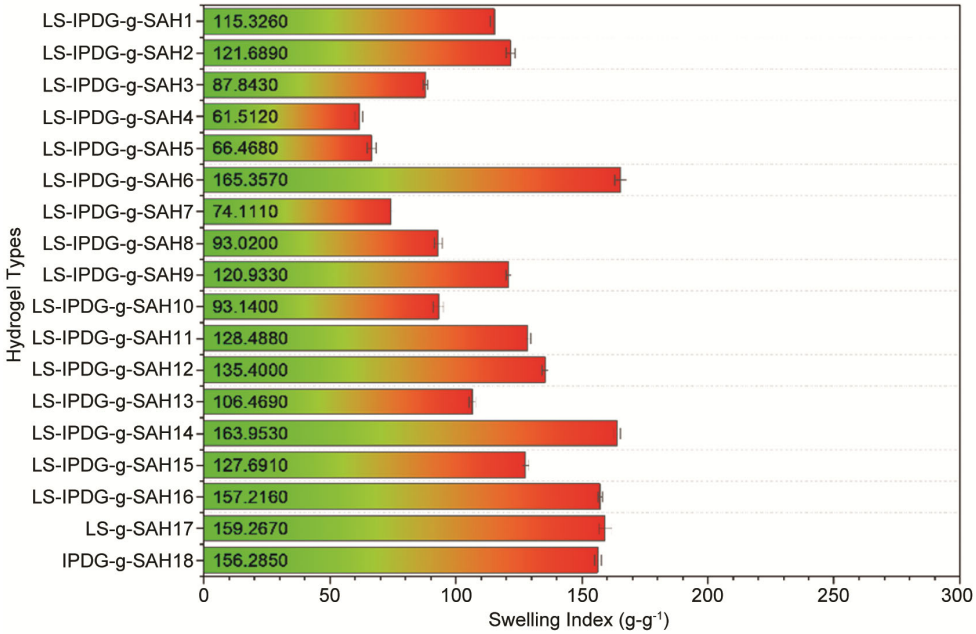

Fig. 8 — Swelling indices for the synthesis of various copolymeric hydrogel formulations

the swelling study results, the synthesized hydrogels exhibited swelling abilities in the following order: LS-IPDG-g-SAH >LS-g-SAH >IPDG-g-SAH. The findings suggest that LS-IPDG-g-SAH contains a greater number of hydrophilic groups and has a lower crosslink density compared to LS-g-SAH and IPDG-g-SAH hydrogels[72]. The swelling results revealed that hydrogels synthesized from IPDG combined with lignin exhibited the highest swelling among all samples. Hydrogels prepared exclusively from LS-grafted AA displayed intermediate swelling, higher than IPDG-only hydrogels but lower than LS-IPDG-g-SAH hydrogels. This highlights the promotion of swelling capacity due to the functionality of highly hydrophilic groups, which can form strong hydrogen bonds with water molecules. Notably, hydrogels with added lignin demonstrated significantly enhanced swelling compared to IPDG-only hydrogels, which showed poor water-holding ability. Therefore, IPDG-only hydrogels are not recommended due to their low water absorption efficiency. Based on the swelling study, among the synthesized samples presented in Fig. 8, LS-IPDG-g-SAH6 exhibited the highest swelling. It was selected as the optimized hydrogel for preparing control samples (LS-g-SAH17 and IPDG-g-SAH18) for further characterization and application studies.

Physical properties of and network parameters LS-IPDG-g-SAH, LS-g-SAH, and IPDG-g-SAH hydrogels

The physical properties, dimensions, and network parameters of various hydrogel formulations were

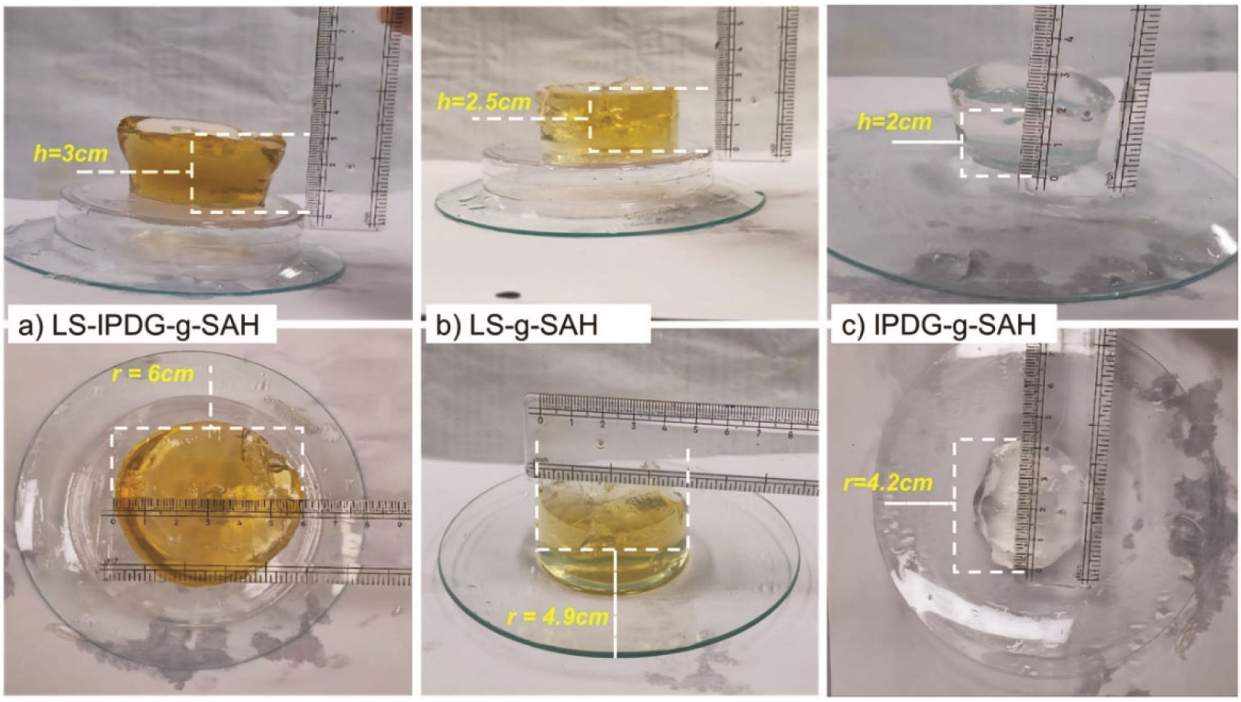

Fig. 9 — Dimensions and colours of various Hydrogel formulations

Table 3 — Calculated values of network parameter of LS-IPDG-g-SAH, LS-g-SAH, and IPDG-g-SAH hydrogels

Hydrogel	Color	X	ϕ	$M_C \times 10^7$ (g.mol^{-1})	ρ ×10^{-9} (mol.mL^{-1})
LS-IPDG-g-SAH	Dark yellow	0.5012	0.00370	17.7954	6.17174
LS-g-SAH	Pale yellow	0.5020	0.00601	8.38677	22.6262
IPDG-g-SAH	Colorless	0.5031	0.00938	3.72556	74.8321

displayed in Fig. 9 and Table 3. Depending on the type and doses of natural precursors, the colours of the gradients of LS-IPDG-g-SAH, LS-g-SAH, and IPDG-g-SAH hydrogels were dark yellow, pale yellow and colourless, respectively. The network parameters provide essential insight into the structure of the chains and the behaviour of hydrogels when absorbing the fluids. The M_C values of LS-IPDG-g-SAH, LS-g-SAH, and IPDG-g-SAH hydrogels were 17.7954×10^7, 8.38677×10^7, and 3.72556×10^7g.mol^{-1}, respectively. The high Mc value indicated that the LS-IPDG-g-SAH hydrogel chains are relatively long, flexible, and lack connections, resulting in the hydrogel swelling more readily upon fluid absorption due to the network's reduced resistance to water penetration. Conversely, the low M_C value indicated that the IPDG-g-SAH hydrogel chains are relatively short, less flexible, and strong connections, resulting in the hydrogel swelling less upon fluid absorption due to the network's increased integrity. The intermediate Mc value of the LS-g-SAH hydrogel exhibited intermediate swelling capacity between the prepared hydrogels, indicating that the M_C results agree with the swelling of the hydrogels. Moreover, the high ρ suggests a higher density and a stronger network of IPDG-g-SAH hydrogels, while the density decreases for LS-g-SAH to 22.6262x10^{-9} (mol. mL^{-1}) and becomes very small for LS-IPDG-g-SAH hydrogel. The mole fraction and hydrogel solvent interaction regularly increase with polymer degree. These behaviours suggest that the hydrogel network expands as the degree of polymerization decreases. A similar behaviour was reported by Dixit *et al.*[73].

Effect of pH on swelling behaviour

The pH is the main factor affecting the swelling ability, as the swelling properties of hydrogels strongly depend on the pH of the solution media, as evident from Figs 10 (a–d). In this work, the swelling properties of the LS-IPDG-g-SAH, LS-g-SAH, and IPDG-g-SAH hydrogels as the optimized sample under varied pH conditions (1.6, 7.2, and 13.1) were investigated by soaking the samples in DW at room temperature. Figs 10 (a–c) show the fluctuations in

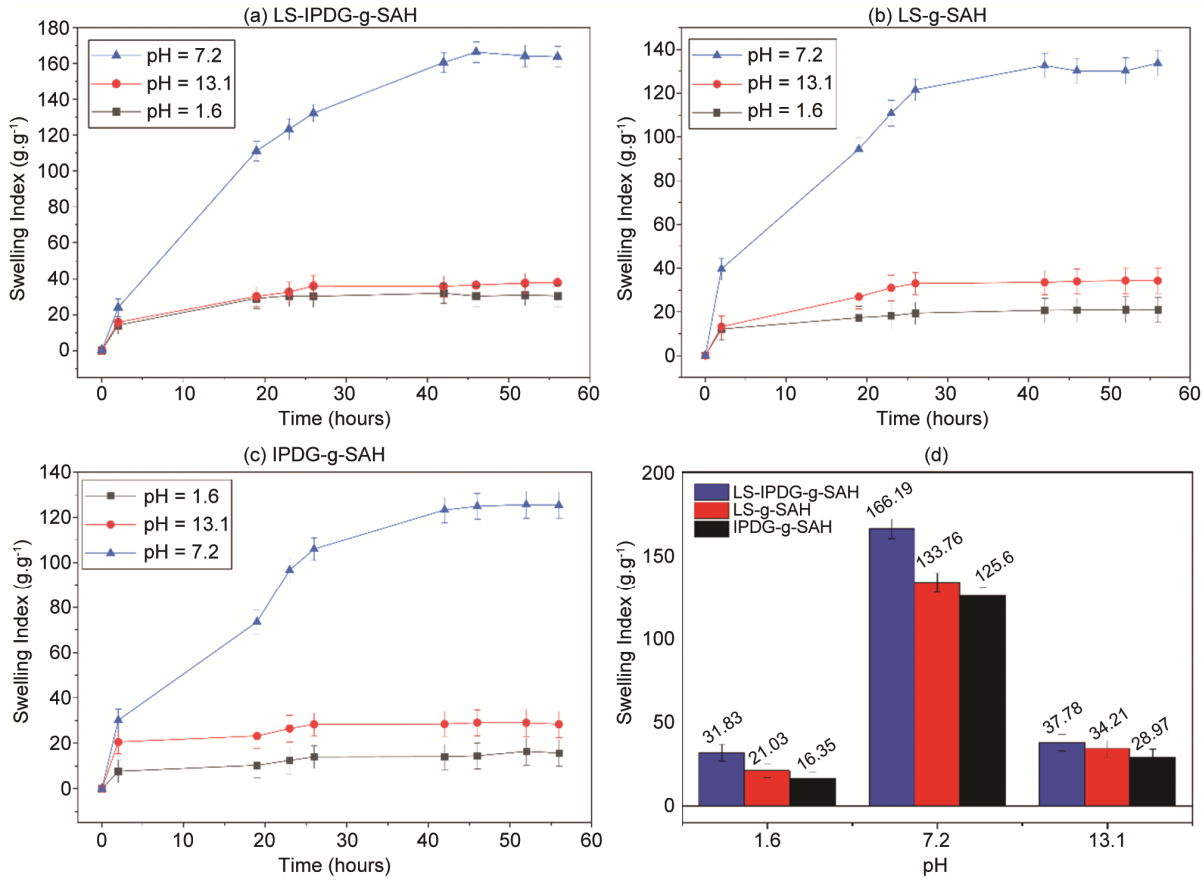

Fig. 10 — SI in different pHs of the concerning time of (a) LS-IPDG-g-SAH, (b) LS-g-SAH, and (c) IPDG-g-SAH hydrogels and (d) comparative equilibrium swelling

swelling capacity as a function of time in different pH conditions. The swelling ratios at pH 1.6, 7.2, and 13.1 were found to be 31.83g.g^{-1}, 166.19 g.g^{-1}, and 37.78 g.g^{-1} for LS-IPDG-g-SAH, 21.03 g.g^{-1}, 133.76 g.g^{-1}, and 34.21g.g^{-1} for LS-g-SAH, and 16.35 g.g^{-1}, 125.6 g.g^{-1}, and 28.97 g.g^{-1} for IPDG-g-SAH hydrogels, respectively. Based on the analysis, the hydrogels showed the maximum SI at pH 7.2 in DW compared to other media. Fig. 10 (d) shows the SI trend, which rises from pH 1.6 to 7.2, then drops to pH 13.1 [74]. At acidic pH (1.6), poor ionization occurs in the cross-linked network of hydrogels, resulting in comparatively less swelling. Thus, water uptake and the electrostatic repulsion between the chains will be dampened by the protonation of carboxyl (–COOH) and other ionizable functional groups in the polymer chain [75]. On the other hand, the generation of negatively charged carboxylate ions (–COO$^-$) in an alkaline medium (pH=13.1) results in a maximum SI and enhanced water penetration and expansion. This is because the deprotonation of functional groups enhances the free volume of the hydrogel network[76]. For example, increased swelling in DW can improve the efficiency of releasing loaded pesticides and agrochemicals with pH-sensitive properties[52,77,78].

Water evaporation analysis

Water evaporation is the process by which water in the soil changes from a liquid to a vapour state, and it increases as the temperature rises, escaping directly from the soil to the atmosphere. Figs 11 (a) and (b) show the water evaporation ratio (WE%) in LS-IPDG-g-SAH, LS-g-SAH, and IPDG-g-SAH treated soils, relative to the untreated blank soil. Soil's capacity to retain water is a critical factor that governs its evaporation rate and enhances its overall water-holding capacity. The maximum evaporation occurred in the blank soil, whereas the minimum value was observed in the LS-IPDG-g-SAH hydrogel-treated soil after 12 days. This is because polymer chains interact with water molecules, along with the restriction of water escape by the macromolecular hydrogel network [79]. As shown in Figs 11 (a) and (b), addition of 1 wt.% of LS-IPDG-g-SAH, LS-g-SAH,

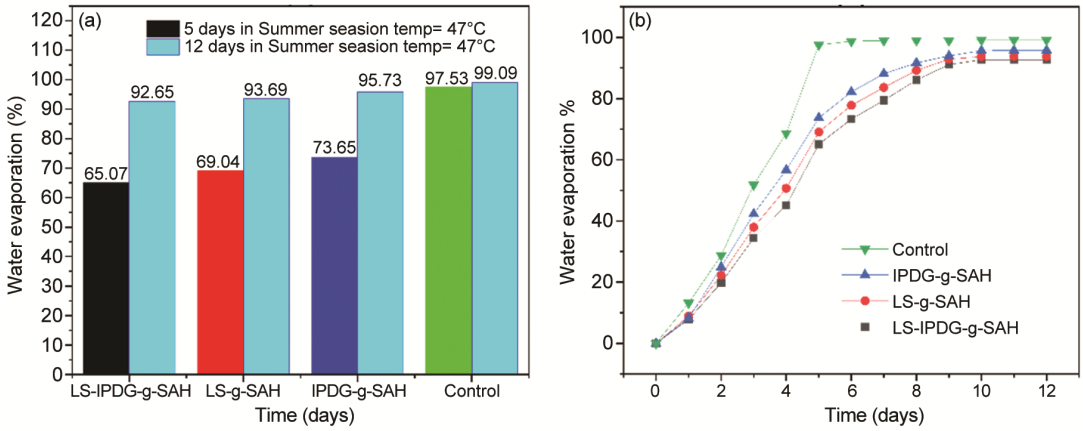

Fig. 11 — Water evaporation study of soil amended with LS-IPDG-g-SAH, LS-g-SAH, IPDG-g-SAH, and control hydrogels: (a) concerning water holding after 5 and 12 days and (b) comparative time

and IPDG-g-SAH hydrogels to control soil (garden soil, DTU, Delhi, India) significantly reduced the rate of evaporation. By the 5th day, the percentages of retained water of LS-IPDG-g-SAH, LS-g-SAH, and IPDG-g-SAH were 65.07%, 69.04%, and 73.65%, respectively, while 97.53% of water had been retained in the blank soil after 5th days. Additionally, the water retention was 92.65% for LS-IPDG-g-SAH, 93.69% for LS-g-SAH, and 95.73% for IPDG-g-SAH, respectively, compared to 99.09% water escape from the blank soil after 12th days. It is worth noting that the experiment was conducted during the summer season, with a maximum temperature of approximately 47°C. Therefore, such severe heat conditions and harsh environmental stress are likely to enhance water evaporation from the soil, thereby highlighting the efficacy of the hydrogel formulations for reducing water loss. The observed trend of water evaporation followed the results of swelling, with LS-IPDG-g-SAH exhibiting the highest swelling, followed by LS-g-SAH and IPDG-g-SAH hydrogels. Interestingly, water evaporation also followed a similar order: Blank soil>IPDG-g-SAH>LS-g-SAH>LS-IPDG-g-SAH. The above order was likely influenced by hindrances among the macromolecular network[79]. After treating the soil with hydrogels, water within the soil is retained for a longer duration, particularly during hot summers[80]. This, in turn, provides more time for water absorption and enhances plant growth, particularly during prolonged drought seasons and stress conditions[81].

Thiamethoxam loading and release kinetics study

In this research, the LE% of the pesticide was calculated for thiamethoxam-loaded synthesized hydrogels. For the hydrogels to be effective in release applications, it should have good loading efficiency to facilitate the slow release over time. The efficiency of loaded synthesized hydrogels of LS-IPDG-g-SAH, LS-g-SAH, and IPDG-g-SAH were determined to be 45.8%, 41.45%, and 39.85%, respectively. The release kinetics of thiamethoxam incorporated into LS-IPDG-g-SAH, LS-g-SAH, and IPDG-g-SAH hydrogel preparations were assessed in DW, which displayed different patterns highly related to the crosslinking density and the structure of the polymeric network. Fig. 12a shows the cumulative release profiles of thiamethoxam from these hydrogels, exhibiting a biphasic process involving a rapid release within the initial hours followed by a slow, sustained release phase characteristic of pesticide delivery systems based on hydrogels. Furthermore, fitting the Korsmeyer–Peppas, Weibull, and Higuchi models provides a comprehensive understanding of the release mechanisms of thiamethoxam, which are illustrated in Figs 12b–12d, and Figs 13a–13c, and 13d–13f, respectively. The Korsmeyer–Peppas model describes drug release by the release exponent. In cylindrical systems, release values between 0–0.45 describe Fickian diffusion, values in the range of 0.45 to 0.89 describe anomalous transport, 0.89 is case II release, and values above 0.89 are super case II transport. Moreover, the release behavior must be less than 60% for the release of pesticides [82]. The Weibull model assigns a time scale or observed rate constant based on the α value and interprets the shape of the release curve in terms of the β value [83]. This model describes drug release from polymeric matrices, where the β value reflects the transport mechanism. A value of β close to 0.75 corresponds to Fickian diffusion. Values of 0.75 and 1 represent a mixed

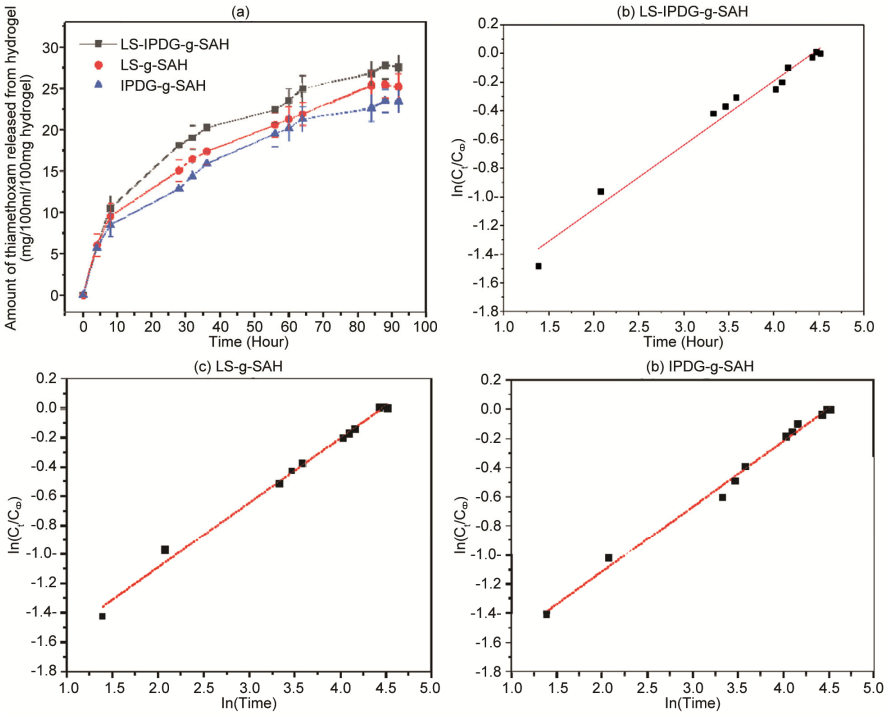

Fig. 12 — Release kinetics of thiamethoxam from hydrogels with respect to time: (a) cumulative amount release and Korsmeyer Peppas model fitting for (b) LS-IPDG-g-SAH, (c) LS-g-SAH, and (d) IPDG-g-SAH hydrogels

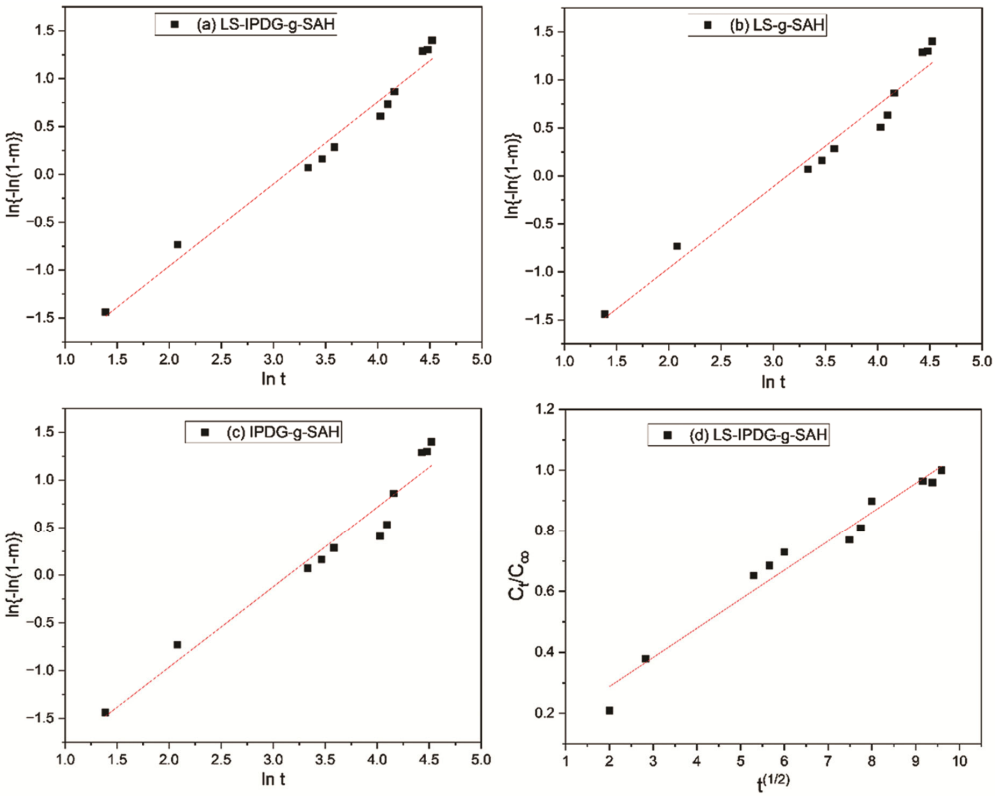

Fig. 13 — Release kinetics of LS-IPDG-g-SAH, LS-g-SAH, and IPDG-g-SAH hydrogels fitted to the Weibull model (a–c) and the Higuchi model (d–f) (*Contd.*)

(*Contd.*)

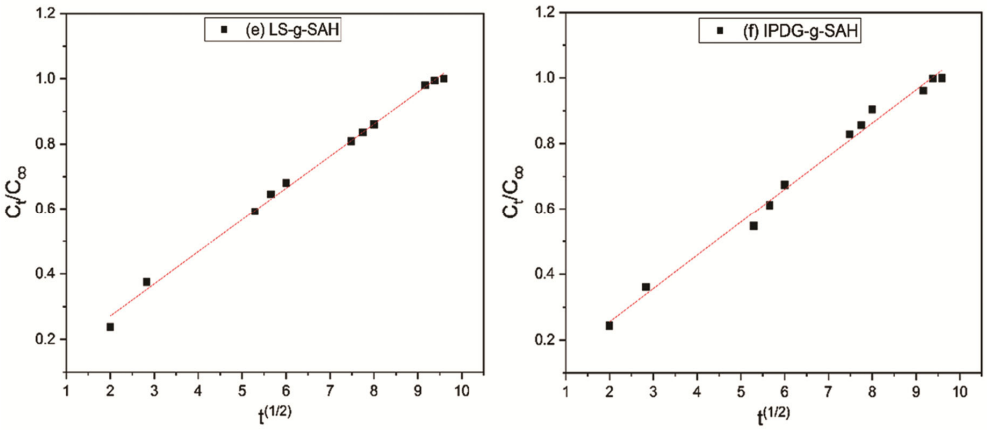

Fig. 13 — Release kinetics of LS-IPDG-g-SAH, LS-g-SAH, and IPDG-g-SAH hydrogels fitted to the Weibull model (a–c) and the Higuchi model (d–f)

Table 4 — Mathematical models studied for the release of thiamethoxam

Formulation	Model	R^2	Parameter	Release Mechanism
LS-IPDG-g-SAH	Korsmeyer-Peppas	0.977	n=0.44691 k=0.1381	Fickian diffusion
	Weibull	0.974	β=0.85732 α=0.0693	Non Fickian behavior
	Higuchi	0.968	K_H=0.09564	Slow diffusion
LS-g-SAH	Korsmeyer-Peppas	0.993	n=0.44278k=0.1386	Fickian diffusion
	Weibull	0.965	β=0.84835α=0.0702	Non Fickian behavior
	Higuchi	0.996	K_H=0.09825	Slow diffusion
IPDG-g-SAH	Korsmeyer-Peppas	0.992	n=0.44897k=0.1335	Fickian diffusion
	Weibull	0.951	β=0.83939α=0.0713	Non Fickian behavior
	Higuchi	0.990	K_H=0.10119	Slow diffusion

mechanism that includes swelling and diffusion, whereas β values higher than 1 reflect more complicated release mechanisms[84]. The release of thiamethoxam is controlled and proceeds along a sequential mechanistic route in the hydrogel products. First, water infiltrates the hydrogel network until the matrix swells. Simultaneously, there is an exchange dynamic of water between the inner hydrogel and the free water in the water. During this period, thiamethoxam repeatedly dissolves and diffuses from the hydrogel matrix, with the release process regulated by osmotic pressure gradients and continued aqueous medium exchange[79]. Under the Korsmeyer–Peppas model, as illustrated in Table 4, the release exponent (n) values fell in the range 0.44278–0.44897. The n values for all hydrogel formulations were below 0.45, describing a Fickian diffusion-controlled process. Furthermore, the strong correlation coefficients ($R^2 > 0.97$) confirm the validity of this model in presenting the release profiles. For the Weibull model, β values ranged from 0.83939 to 0.85732, exceeding 0.75, which is indicative of a diffusion-controlled (non-Fickian) release mechanism for all formulations. The excellent fit of the model to the release data is also verified by the high correlation coefficients ($R^2 > 0.95$).The Higuchi model also accounted for a strongly correlated ($R^2 > 0.96$), indicating the prevalence of diffusion as a regulating mechanism. The K_H values were low, indicating controlled and slower diffusion of thiamethoxam from the synthesized hydrogel networks. Therefore, the study identifies diffusion as the significant mechanism for all preparations, with minor variations due to the impact of polymer composition and structural adjustments. It was suggested that adding IPDG to LS enhances the release behaviour by adjusting the interaction between diffusion and swelling, thereby imparting improved control over the release profile.

Conclusion

The current research presents novel hydrogels successfully synthesized from an Iraqi *Prunus domestica* gum and lignosulfonic acid sodium

saltformulationusing free radical copolymerization. Based on the swelling investigation, the optimized hydrogels exhibited a maximum absorption capacity(165.357±2.331 $g.g^{-1}$) at swelling equilibrium and demonstrated excellent swelling ability in distilled water within varying pH conditions after 60 h. Characterizations showed that the prepared samples have the appropriate structural integrity, porosity, and thermal stability. Furthermore, the strategic interactions between these natural precursors enhanced absorption efficiency, as the polyphenolic compounds positively improved hydrophilicity, compared to the individual formulations. Their applications for the controlled release of thiamethoxam enhanced the performance of the pesticide. It was also emphasized that the potential to offer prolonged release, enhance pesticide efficacy, reduce environmental degradation, and resolve the pivotal issue of pesticide runoff. These findings and enhancements propose the hydrogels as effective vehicles for the controlled release of agrochemicals, providing a feasible and eco-friendly alternative that addresses the shortcomings of gum-only hydrogels. This research provides a solid foundation and novel strategies for developing advanced hydrogel systems for agrochemical applications in modern agriculture to enhance soil fertility by adding multifunctional natural material-based hydrogels to the soil, providing significant importance in the field of potential agricultural development. Future studies recommend using duplicate and triplicate new resources of natural precursors to identify excellent agrochemical applications, overcoming various challenges on a global scale.

Conflict of Interest

The authors declare that they have no conflict of interest.

Acknowledgements

The authors are thankful to the Institute of Pesticide Formulation and Technology, Gurugram, for providing the thiamethoxam. The authors sincerely thank the Department of Applied Chemistry at Delhi Technological University, Delhi, for providing the laboratory facilities used in this research.

References

1 Piccoli I, Camarotto C, Squartini A, Longo M, Gross S, Maggini M, Cabrera M L & Morari F, Hydrogels for agronomical application, *Agron Sustain Dev*, 44 (2024) 22.

2 Qin C, Wang H, Zhao Y, Qi Y, Wu N, Zhang S & Xu W, Recent advances of hydrogel in agriculture: Synthesis, mechanism, properties and applications, *Eur Polym J*, 219 (2024) 113376.

3 Tariq Z, Iqbal D N, Rizwan M, Ahmad M, Faheem M & Ahmed M, Significance of biopolymer-based hydrogels and their applications in agriculture: A review in perspective of synthesis and their degree of swelling for water holding, *RSC Adv*, 13 (2023) 24731.

4 Arafa E G, Sabaa M W, Mohamed R R, Elzanaty A M & Abdel-gawad O F, Preparation of biodegradable sodium alginate / carboxymethylchitosan hydrogels for the slow-release of urea fertilizer and their antimicrobial activity, *React Funct Polym*, 174 (2022) 105243.

5 Zheng L, Seidi F, Liu Y, Wu W & Xiao H, Polymer-based and stimulus-responsive carriers for controlled release of agrochemicals, *Eur Polym J*, 177 (2022) 111432.

6 Berradi A, Aziz F, El-Achaby M, Ouazzani N & Mandi L, A comprehensive review of polysaccharide-based hydrogels as promising biomaterials, *Polymer*, 15 (2023) 2908.

7 Sanjanwala D, Londhe V, Trivedi R, Bonde S, Sawarkar S, Kale V & Patravale V, Polysaccharide-based hydrogels for medical devices, implants and tissue engineering: A review, *Int J Biol Macromol*, 256 (2024) 128488.

8 Ali K, Asad Z, Agbna G H D, Saud A, Khan A & Zaidi S J, Progress and innovations in hydrogels for sustainable agriculture, *Agronomy*, 14 (2024) 2815.

9 Henn G S, Schmitz C, Fontana L B, Corrêa H V N, Lehn D N & de Souza C F V, Water absorption capacity and agricultural utility of biopolymer-based hydrogels: A systematic review and meta-analysis, *ACS Polym Au*, 5 (2025) 325.

10 Chamorro A F, Palencia M & Combatt E M, Starch hydrogels for slow and controlled-release fertilizers: A review, *Polymer*, 17 (2025) 1117.

11 Chaudhary R, Kumar S & Sharma V, Agricultural biowaste valorization towards circular economy: Nanoparticles synthesis and biopolymers extraction for wastewater remediation, *Biores Technol Rep*, 32 (2025) 102357.

12 Guo L, Wang Y, Wang M, Shaghaleh H & Alhaj Y, Synthesis of bio-based MIL-100 (Fe)@ CNF-SA composite hydrogel and its application in slow-release N-fertilizer, *J Clean Prod*, 324 (2021) 129274.

13 Gil-ortiz R, Naranjo M Á, Ruiz-Navarro A, Atares S, Garc C, Zotarelli L, Bautista A S & Vicente O, Enhanced agronomic efficiency using a new controlled-released, polymeric-coated nitrogen fertilizer in rice, *Plan*, 9 (2020) 1183.

14 Sharma A, Bhushette P R & Annapure U S, Purification and physicochemical characterization of Prunus domestica exudate gum polysaccharide, *Carbohydr Polym Technol Appl*, 1 (2020) 100003.

15 Mehmood S, Hasan S M F, Noor R, Sikandar M, ul Hasan M S N, Israr F, Ali S I, Ullah M & Hassan F, Influence of Prunus domestica gum on the release profiles of propranolol HCl floating tablets, *PLoS One*, 17 (2022) e0271442.

16 Han-Min W, Yuan T Q, Song G Y & Sun R C, Advanced and versatile lignin-derived biodegradable composite film materials toward a sustainable world, *Green Chem*, 23 (2021) 3790.

17 Chelliah R, Wei S, Vijayalakshmi S, Barathikannan K, Sultan G, Liu S & Oh D H, A comprehensive mini-review on

lignin-based nanomaterials for food applications: Systemic advancement and future trends, *Molecular*, 28 (2023) 6470.
18 Trishkin G N, Chernysheva M G, Kulikova N A & Badun G A, Eco-friendly polysaccharides as moisture retainers: influence on humic acid colloidal stability in model and natural systems, *Molecules*, 30 (2025) 3618.
19 Noureen S, Noreen S, Ghumman S A, Abdelrahman E A, Batool F, Aslam A, Mehdi M, Shirinfar B & Ahmed N, A novel pH-responsive hydrogel system based on Prunus armeniaca gum and acrylic acid: Preparation and evaluation as a potential candidate for controlled drug delivery, *Eur J Pharm Sci*, 189 (2023) 106555.
20 Kamran M, ul Haq A S A, Rahman G & Bilal S, Potential impacts of prunus domestica based natural gum on physicochemical properties of polyaniline for corrosion inhibition of mild and stainless steel, *Polym*, 14 (2022) 3116.
21 Manu, Gupta R K & Kumar D, Synthesis, characterization and application of Lignosulphonate-g- poly(sodium acrylate) hydrogel, *Indian J Chem Technol*, 30 (2023) 753.
22 Venezia V, Avallone P R, Vitiello G, Silvestri B, Grizzuti N, Pasquino R & Luciani G, Adding humic acids to gelatin hydrogels: A way to tune gelation, *Biomacromolecules*, 23 (2022) 443.
23 Yadav P, Warkar S G & Kumar A, Fabrication of carboxymethyl tamarind kernel gum-based pH-responsive hydrogel composite for oral delivery of azithromycin drug, *Int J Biol Macromol*, 322 (2025) 146662.
24 Naeem F, Khan S, Jalil A, Ranjha N M, Riaz A & Haider M S, pH responsive cross-linked polymeric matrices based on natural polymers : Effect of process variables on swelling characterization and drug delivery properties, *Tabriz Univ Med Sci*, 7 (2017) 177.
25 Larran E, Im M, Toh J X, Irwin N J, Ripolin A, Perminova A, Dom J, Rodr A & Donnelly R F, Synthesis and characterization of lignin hydrogels for potential applications as drug eluting antimicrobial coatings for medical materials, *ACS Sustain Chem Eng*, 6 (2018) 9037.
26 Majid S, Bukhari H, Khan S, Rehanullah M & Ranjha N M, Synthesis and characterization of chemically cross-linked acrylic acid / gelatin hydrogels: Effect of ph and composition on swelling and drug release, *Int J Polym Sci*, 2015 (2015) 1.
27 Roy A, Roy M, Alghamdi S, Dablool A S, Almakki A A, Ali I H, Yadav K K, Islam M R & Cabral-Pinto M M S, Role of microbes and nanomaterials in the removal of pesticides from wastewater, *Int J Photoenergy*, 2022 (2022) 2131583.
28 Raafat A I, Eid M & El-Arnaouty M B, Radiation synthesis of superabsorbent CMC based hydrogels for agriculture applications, *Nucl Instrum Methods Phys Res Sect B Beam Interact Mater Atoms*, 283 (2012) 71.
29 Elabasy A, Shoaib A, Waqas M, Shi Z & Jiang M, Cellulose nanocrystals loaded with thiamethoxam: Fabrication, characterization, and evaluation of insecticidal activity against phenacoccus solenopsis tinsley (Hemiptera: Pseudococcidae), *Nanomaterial*, 10 (2020) 788.
30 Dharmalingam K & Anandalakshmi R, Fabrication, characterization and drug loading efficiency of citric acid crosslinked NaCMC-HPMC hydrogel films for wound healing drug delivery applications, *Int J Biol Macromol*, 134 (2019) 815.
31 Baglioni M, Clemente I, Tamasi G, Bisozzi F, Costantini S, Fattori G, Gentile M & Rossi C, Isothiocyanate-based microemulsions loaded into biocompatible hydrogels as innovative biofumigants for agricultural soils, *Molecules*, 29 (2024) 3935.
32 Kowalski G, Witczak M & Kuterasiński Ł, Structure effects on swelling properties of hydrogels based on sodium alginate and acrylic polymers, *Molecules*, 29 (2024) 1937.
33 Khushbu, Warkar S G & Kumar A, Synthesis and assessment of carboxymethyl tamarind kernel gum based novel superabsorbent hydrogels for agricultural applications, *Polymer*, 182 (2019) 121823.
34 Srivastava A, Nandal M & Gupta R K, Xanthan gum and lignin grafted chemically crosslinked hydrogels for dye removal: Synthesis, characterization and isotherms studies, *Polym Sci Ser A*, 65 (2023) 725.
35 Ganguly S, Mondal S, Das P, Bhawal P, Maity P P, Ghosh S, Dhara S & Das N C, Design of psyllium-g-poly(acrylic acid-co-sodium acrylate)/cloisite 10A semi-IPN nanocomposite hydrogel and its mechanical, rheological and controlled drug release behaviour, *Int J Biol Macromol*, 111 (2018) 983.
36 Liu L, Sawut A, Abliz S, Nurulla I, Dolat B & Yimit M, Ultraviolet-induced polymerization of superabsorbent composites based on sodium humate and its urea release behavior, *RSC Adv*, 6 (2016) 101123.
37 Ni B, Liu M & Lü S, Multifunctional slow-release urea fertilizer from ethylcellulose and superabsorbent coated formulations, *Chem Eng J*, 155 (2009) 892.
38 Rahim H, Khan M A, Badshah A, Chishti K A, Khan S & Junaid M, Evaluation of Prunus domestica gum as a novel tablet binder, *Braz J Pharm Sci*, 50 (2014) 195.
39 Li Z, Kong Y & Ge Y, Synthesis of porous lignin xanthate resin for Pb2+ removal from aqueous solution, *Chem Eng J*, 270 (2015) 229.
40 Karpukhina E A, Volkov D S & Proskurnin M A, Quantification of lignosulfonates and humic components in mixtures by ATR FTIR spectroscopy, *Agronomy*, 13 (2023) 1141.
41 Deore U V & Mahajan H S, Isolation and structural characterization of mucilaginous polysaccharides obtained from the seeds of Cassia uniflora for industrial application, *Food Chem*, 351 (2021) 129262.
42 Shi L, Liu W, Zhang X & Hu J, Preparation of lignin sulfonate based/organo-montmorillonite composite hydrogel for adsorbing methylene blue from aqueous solution, *J Polym Environ*, 30 (2022) 4287.
43 Benhadria N, Hachemaoui M, Zaoui F, Mokhtar A, Boukreris S, Attar T, Belarbi L & Boukoussa B, Catalytic reduction of methylene blue dye by copper oxide nanoparticles, *J Clust Sci*, 33 (2022) 249.
44 Raschip I E, Hitruc G E, Vasile C & Popescu M C, Effect of the lignin type on the morphology and thermal properties of the xanthan/lignin hydrogels, *Int J Biol Macromol*, 54 (2013) 230.
45 Temel S, Gokmen F O & Yaman E, Antibacterial activity of ZnO nanoflowers deposited on biodegradable acrylic acid hydrogel by chemical bath deposition, *Bull Mater Sci*, 43 (2020) 18.
46 Nandal M, Prashar V, Bansiwal M, Kapoor I, Kansal T & Gupta R K, Novel molasses-grafted poly(sodium acrylate) hydrogel: A sustainable solution for water retention and controlled dinotefuran release, *Indian J Chem Technol*, 32 (2025) 161.

47 Bahrpaima K & Fatehi P, Preparation and coagulation performance of carboxypropylated and carboxypentylated lignosulfonates for dye removal, *Biomolecules*, 9 (2019) 383.

48 Hawkes G E, Smith C Z, Utley J H P, Vargas R R & Viertler H, A comparison of solution and solid state 13C NMR spectra of lignins and lignin model compounds, *Holzforschung*, 47 (1993) 302.

49 Petrea P, Amarioarei G, Apostolesco N, Puitel A D & Ciovica S, Some aspects of the characterization of vegetable gums: Prunus persica (Plum) and prunus domestica (Cherry), *Cellul Chem Technol*, 47 (2013) 369.

50 Tanwar M, Gupta R K & Rani A, Carboxymethylated gum tragacanth crosslinked poly(sodium acrylate)hydrogel: Fabrication, characterization, rheology and drug-delivery application, *Indian J Chem Technol*, 30 (2023) 308.

51 Neppel A, Eaton D R, Hunkeler D & Hamielec A E, Effect of crosslinking on the 13C nuclear magnetic resonance spectra of superabsorbent poly(sodium acrylates), *Polymer*, 29 (1988) 1338.

52 Balodhi D, Khushbu, Warkar S G, Rani A & Gupta R K, Natural carbohydrate gums based hydrogels, *Indian J Chem Technol*, 28 (2021) 262.

53 Jabrail F H, Mutlaq M S & Al-Ojar R K, Studies on agrochemical controlled release behavior of copolymer hydrogel with PVA Blends of natural polymers and their water-retention capabilities in agricultural soil, *Polymers*, 15 (2023) 3545.

54 Song B, Liang H, Sun R, Peng P, Jiang Y & She D, Hydrogel synthesis based on lignin/sodium alginate and application in agriculture, *Int J Biol Macromol*, 144 (2020) 219.

55 Erceg T, Cakić S, Cvetinov M, Dapčević-Hadnađev T, Budinski-Simendić J & Ristić I, The properties of conventionally and microwave synthesized poly(acrylamide-co-acrylic acid) hydrogels, *Polym Bull*, 77 (2020) 2089.

56 Chavda H & Patel C, Effect of crosslinker concentration on characteristics of superporous hydrogel, *Int J Pharm Investig*, 1 (2011) 17.

57 Darban Z, Shahabuddin S, Gaur R, Ahmad I & Sridewi N, Hydrogel-based adsorbent material for the effective removal of heavy metals from wastewater: A comprehensive review, *Gels*, 8 (2022) 263.

58 Aljeboree A M, Alkaim A F, Hussein S A, Jawad M A, Hasan I & Khuder S A, Synthesis and swelling behavior of highly adsorbent hydrogel for the removal of brilliant green from an aqueous solution: Thermodynamic, kinetic, and isotherm models, *Case Stud Chem Environ Eng*, 10 (2024) 100831.

59 Elsayed A E, Attia S K, Rashad A M, Mahmoud G A & Osman D I, Synthesis of dispersed magnetic Fe_3O_4 nanohydrogel based on gelatine by gamma irradiation for toxic heavy metals removal, *J Inorg Organomet Polym Mater*, 35 (2025) 2546.

60 Santos A, Bertoli A, Borges A C, Gomes R, Garcia J & Trevisan M, New organomineral complex from humic substances extracted from poultry wastes: Synthesis, characterization and controlled release study, *J Braz Chem Soc*, 29 (2018) 140.

61 Bora A & Karak N, Starch and itaconic acid-based superabsorbent hydrogels for agricultural application, *Eur Polym J*, 176 (2022) 111430.

62 Komisarz K, Majka T M & Pielichowski K, Chemical transformation of lignosulfonates to lignosulfonamides with improved thermal characteristics, *Fibers*, 10 (2022) 20.

63 Mun S P, Cai Z & Zhang J, Fe-catalyzed thermal conversion of sodium lignosulfonate to graphene, *Mater Lett*, 100 (2013) 180.

64 Maharjan B, Park J, Kaliannagounder V K, Awasthi G P, Joshi M K, Park C H & Kim C S, Regenerated cellulose nanofiber reinforced chitosan hydrogel scaffolds for bone tissue engineering, *Carbohydr Polym*, 251 (2021) 117023.

65 Ji X, Guo M, Zhu L, Du W & Wang H, Synthesis mechanism of an environment-friendly sodium lignosulfonate/chitosan medium-density fiberboard adhesive and response of bonding performance to synthesis mechanism, *Materials*, 13 (2020) 5697.

66 Gaisin R A, Imayev V M & Imayev R M, Effect of hot forging on microstructure and mechanical properties of near α titanium alloy/TiB composites produced by casting, *J Alloys Compd*, 723 (2017) 385.

67 Bosworth L A, Rathbone S R, Bradley R S & Cartmell S H, Dynamic loading of electrospun yarns guides mesenchymal stem cells towards a tendon lineage, *J Mech Behav Biomed Mater*, 39 (2014) 175.

68 Adnadjevic B & Jovanovic J, Novel approach in investigation of the poly(acrylic acid) hydrogel swelling kinetics in water, *J Appl Polym Sci*, 107 (2008) 3579.

69 Rop K, Mbui D, Karuku G N, Michira I & Njomo N, Characterization of water hyacinth cellulose-g-poly (ammonium acrylate-co-acrylic acid)/nano-hydroxyapatite polymer hydrogel composite for potential agricultural application, *Results Chem*, 2 (2020) 100020.

70 Nandal M, Kumar D & Gupta R K, Novel formulations of humic acid, lignin, and lignite grafted hydrogels for the slow release of thiamethoxam, *CheistrySelect*, 9 (2024) e202304939.

71 Kim J K, Choi B & Jin J, Transparent, water-stable, cellulose nanofiber-based packaging film with a low oxygen permeability, *Carbohydr Polym*, 249 (2020) 116823.

72 Hoti G, Caldera F, Cecone C, Rubin-Pedrazzo A, Anceschi A, Appleton S L, Khazaei-Monfared Y & Trotta F, Effect of the cross-linking density on the swelling and rheological behavior of ester-bridged β-cyclodextrin nanosponges, *Materials*, 14 (2021) 478.

73 Dixit A, Bag D S, Sharma D K, Singh H & Prasad N E, Effect of crosslinking on the network parameters, swelling and mechanical properties of PVA-borax and poly (AM-co-HEMA) double network (DN) *Hydrogels*, *J Polym Mater*, 35 (2018) 371.

74 Mohamed S F, Mahmoud G A & Taleb M F A, Synthesis and characterization of poly(acrylic acid)-g-sodium alginate hydrogel initiated by gamma irradiation for controlled release of chlortetracycline HCl, *Monatshefte für Chemie Chem Mon*, 144 (2013) 129.

75 Khan S, Babadaei M M N, Hasan A, Edis Z, Attar F, Siddique R, Bai Q, Sharifi M & Falahati M, Enzyme-polymeric/inorganic metal oxide/hybrid nanoparticle bio-conjugates in the development of therapeutic and biosensing platforms, *J Adv Res*, 33 (2021) 227.

76 Wu M, Niu X, Zhang R & Xu Z P, Two-dimensional nanomaterials for tumor microenvironment modulation and anticancer therapy, *Adv Drug Deliv Rev*, 187 (2022) 114360.

77 Zhang M, Zhang X, Huang S, Cao Y, Guo Y & Xu L, Programmed nanocarrier loaded with paclitaxel and dual-siRNA to reverse chemoresistance by synergistic therapy, *Int J Biol Macromol*, 261 (2024) 129726.

78 Ferreira S S, Correia A, Silva A M S, Wessel D F, Cardoso S M, Vilanova M & Coimbra M A, Structure-function relationships of pectic polysaccharides from broccoli by-products with in vitro B lymphocyte stimulatory activity, *Carbohydr Polym*, 303 (2023) 120432.

79 Rabat N E, Hashim S & Majid R A, Effect of different monomers on water retention properties of slow release fertilizer hydrogel, *Procedia Eng*, 148 (2016) 201.

80 Palma D, Lagos O, Souto C, Pérez A, Quezada L, Hirzel J, Vera M, Ulloa J & Urbano B, Evaluation of a natural superabsorbent polymer on water retention capacity in coarse-textured soils, *Water*, 16 (2024) 3186.

81 Rajanna G A, Manna S, Singh A, Babu S, Singh V K, Dass A, Chakraborty D, Patanjali N, Chopra I, Banerjee T, Kumar A, Khandelwal A & Parmar B S, Biopolymeric superabsorbent hydrogels enhance crop and water productivity of soybean-wheat system in indo-gangetic plains of India, *Sci Rep*, 12 (2022) 11955.

82 Costa P & Sousa-Lobo J M, Evaluation of mathematical models describing drug release from estradiol transdermal systems, *Drug Dev Ind Pharm*, 29 (2003) 89.

83 Alam M A, Takafuji M & Ihara H, Silica nanoparticle-crosslinked thermosensitive hybrid hydrogels as potential drug-release carriers, *Polym J* , 46 (2014) 293.

84 Paolino D, Tudose A, Celia C, Di-Marzio L, Cilurzo F & Mircioiu C, Mathematical models as tools to predict the release kinetic of fluorescein from lyotropic colloidal liquid crystals, *Materials*, 12 (2019) 693.